Article published online: 2022-02-24

Rubidium Uptake in Chest Tumors on PET/CT

Jorge D. Oldan[1] Abiola D. Femi-Abodunde[1] Mitchel A. Muhleman[1] Amir H. Khandani[1]

[1] Department of Radiology, University of North Carolina, Chapel Hill, North Carolina, United States

World J Nuclear Med 2022;21:18–27.

Address for correspondence Jorge D. Oldan, MD, Department of Radiology, University of North Carolina, Chapel Hill, North Carolina, 27514, United States (e-mail: joldan9@gmail.com).

Abstract

Background Chest tumors are often found incidentally on cardiac scans; we aimed to describe the findings of rubidium (Rb) in incidentally discovered extracardiac tumors.

Materials and Methods We reviewed a database of cardiac Rb scans performed over a period of 11 years and identified those with a previously unsuspected malignancy seen on the plane of section. We then measured maximum standard uptake value for each of the tumors, as well as background lung, liver, mediastinum, and body wall. In cases where fluorodeoxyglucose (FDG) positron emission tomography (PET)/computed tomography (CT) was available, we compared Rb results with FDG PET/CT.

Results We identified 63 patients meeting criteria including full visualization of a tumor of at least 1.0 cm with no prior treatment. Of these patients, 17 had breast, 36 had lung, and 10 had miscellaneous other tumors. We selected patients with either breast or lung tumors for further analysis. Overall uptake was relatively stable between rest and stress but lower than FDG PET/CT; it was generally low and similar to blood pool. There was a small but statistically significant correlation between estrogen receptor positivity and Rb uptake in breast tumors. There was a stable pattern of uptake in background tissues, with liver being greater than mediastinal blood pool, which in turn was more avid than lung, which was more avid than subcutaneous body wall tissues. Lung showed a noticeable tendency toward increased uptake in dependent regions, likely reflecting low-level atelectasis.

Conclusion Uptake was stable between rest and stress but low relative to FDG PET/CT; some correlations with receptors suggest it may be useful in molecular imaging.

Keywords
- PET/CT
- rubidium
- oncology
- chest

Introduction

Rubidium-82 chloride (^{82}Rb) is a common myocardial perfusion imaging agent moved into myocytes by the sodium–potassium transporter and often used to diagnose ischemia and infarction.[1] Malignancies such as brain tumors,[2,3] malignant and metastatic pheochromocytoma,[4,5] and breast metastases and aggressive prostate cancers also take up ^{82}Rb,[6,7] and are incidentally detected in approximately 2% of cardiac scans.[8] We reported visual comparisons of tumors to background and semiquantitative analysis of uptake, and now aim to confirm our previous results in breast and lung tumors (the most common) and assess possible molecular imaging applications.[1]

DOI https://doi.org/10.1055/s-0042-1744195.
ISSN 1450-1147.

Thieme Medical and Scientific Publishers Pvt. Ltd., A-12, 2nd Floor, Sector 2, Noida-201301 UP, India

Materials and Methods

Selection and Description of Participants

We first obtained Institutional Review Board (IRB) (ethics committee) approval and ensuring Health Insurance Portability and Accountability Act compatibility for this retrospective study. IRB study number was 18-1137, approved May 2, 2018. Patient consent was waived under exemption for minimal risk in this retrospective study.

We then acquired the names and medical record numbers of all patients who had a cardiac ^{82}Rb PET/computed tomography (CT) at our institution from July 1, 2007, to July 1, 2018, and a new diagnosis of breast or lung cancer within 60 days from each other. There were a total of 509 patients, of whom 120 had a malignant lesion within the Rb PET/CT field of view, which extended roughly from the aortic arch to the liver to provide attenuation correction. (Note that this is significantly higher than the usual overall rate of incidentally discovered lesions of approximately 2%,[8] as patients were specifically selected for having a new diagnosis of breast or lung cancer within 60 days of the scan.) A total of 63 cases fulfilled the following criteria, and were therefore investigated further: (1) the entire lesion was captured on both stress and rest images; (2) the lesion had a size of at least 1.0 cm, the usual lower limit for visibility by PET/CT, to minimize partial volume effects; (3) histologic diagnosis was available in the electronic medical record system; and (4) the patient had not been previously treated by chemotherapy, radiation, or surgery. From these 63 cases, the most common tumor types were breast (17 cases) and lung (36 cases). Other tumors found included four lymphomas, two esophageal tumors, a carcinoid of the lung, a carcinosarcoma of the ovary, and lung metastases from gastrointestinal (GI) adenocarcinoma and clear cell renal carcinoma. Given the small numbers of other tumors, we only selected the 53 breast and lung tumors for further analysis. (We describe uptake of the other 10 tumors in the Results for reference.) Tumor type was determined from histopathology. Given the fact that a diagnosis of cancer was one of the criteria for selection, there were relatively few benign lesions, and these were not selected for further work-up. The lung lesions selected for further analysis were primary lung lesions; the two metastatic lung lesions mentioned earlier were not selected for further work-up.

Technical Information

PET/CT Data Acquisition and Processing and Image Review

As previously described,[1] our routine cardiac ^{82}Rb PET/CT protocol includes a rest PET/CT scan followed by a stress PET/CT scan after pharmacologic stress with 0.4 mg of intravenous regadenoson (Lexiscan) (Astellas US LLC, Northbrook, Illinois, United States). The patients were scanned using either a Biograph mCT 128-slice scanner or a Biograph TruePoint 40-slice (Siemens Healthcare, Malvern, Pennsylvania, United States). We acquire for 8 minutes in list mode, starting at the completion of ^{82}Rb infusion. Because of the presence of ^{82}Rb in the background and its ongoing uptake in the myocardium, the first 90 seconds were not used for image reconstruction; the remaining 390 seconds were reconstructed as a static image with vendor-provided software, using ordered subsets expectation maximization (OSEM) (2 iterations and 24 subsets) three-dimensional reconstruction with a 6.5-mm Gaussian postprocessing filter. Both portions of the examination used an intravenous dose of 1,480 MBq of ^{82}Rb, using a Cardiogen strontium-82 (82Sr)/^{82}Rb generator (Bracco Diagnostics, Monroe Township, New Jersey, United States). Shallow-breathing low-dose (120 kVp; 50 mAs) CT scans were acquired before the rest portion and after the stress portion of the examination for attenuation correction. The radiologist routinely reviewed these scans to assess for coronary calcification and other incidental findings, such as lung nodules.

Where an F18-fluorodeoxyglucose (FDG) PET/CT image obtained within a month was available, this was also included. FDG PET/CT scans were acquired using either a Biograph TruePoint 40-slice or Biograph mCT 128-slice scanner (Siemens Healthcare). Examination was done using 259 to 740 MBq of ^{18}F-FDG using a weight-based formula, and 2 minutes per bed position for the TruePoint and 1.5 minutes per bed position for the mCT. CT parameters were 100 mAs and 120 kVp. Reconstruction used an OSEM algorithm (two iterations eight subsets) with 5-mm Gaussian filter and matrix of 168×168 (TruePoint) or 200×200 (mCT).

Lesion Selection

In each of the 53 cases included in this study, we used the most avid malignant lesion captured on ^{82}Rb PET/CT images for visual, semiquantitative, and quantitative analyses. If the same lesion was visible on an FDG PET/CT as described earlier, we obtained maximum standard uptake value (SUVmax) on that scan as well for comparison.

Visual Analysis

Two nuclear medicine physicians (reader 1 and reader 2) with extensive PET/CT imaging experience reviewed the ^{82}Rb rest and stress images independently, using MIM (MIM Software Inc, Cleveland, Ohio, United States) oncology review workflows. The uptake in each lesion was compared with uptake of subcutaneous fat, lung, mediastinal blood pool, liver, and apparently healthy myocardium and scored as follows, based on our previous publication[1]: (1) equal or greater to subcutaneous fat but less than lung; (2) greater than lung but less than or equal to MBP; (3) greater than MBP but less than or equal to liver; and (4) greater than liver but less than heart. Examples of breast and lung lesions are shown in ►**Figs. 1** and **2**.

Quantitative Analysis

Reader 1 quantitatively assessed uptake in the malignant lesions on ^{82}Rb PET/CT and FDG PET/CT at a different time point than visual analysis, using SUV_{max}. This is the most commonly used quantitative method of assessing uptake due to reproducibility, particularly where dynamic data such as arterial input functions are not available. SUV_{max} of each

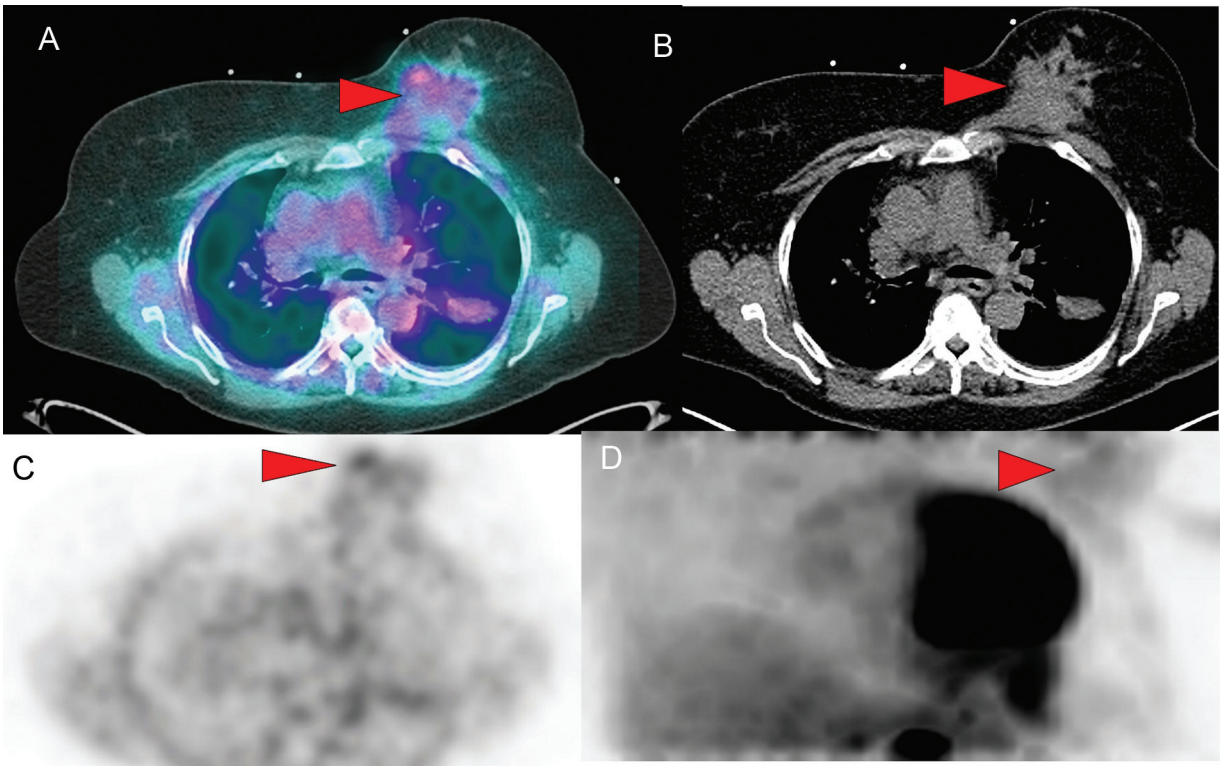

Fig. 1 (**A–D**) Left breast lesion on stress image (*red arrowhead*), similar in avidity to mediastinal blood pool; notice the relatively high avidity of mediastinal blood pool.

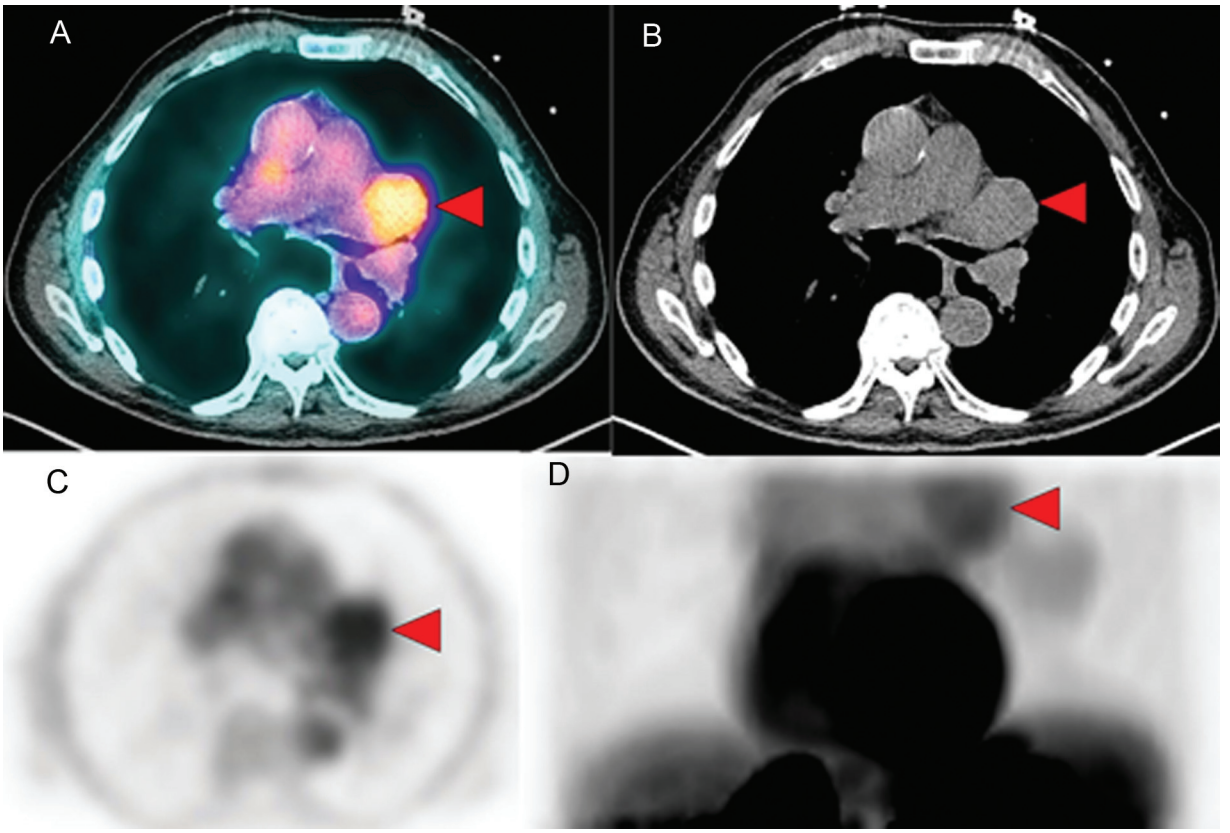

Fig. 2 (**A–D**) Left lung lesion adjacent to mediastinum (*red arrowhead*) on stress image, significantly more avid than mediastinal blood pool and lung.

malignant lesion was calculated by placing a three-dimensional region of interest (ROI) around the most intense area in the lesion on rest and stress ^{82}Rb PET/CT, and FDG images (SUV_{rest}, SUV_{stress}, and SUV_{FDG}, respectively). SUV_{max} in subcutaneous fat (SUV_{fat}), lung (SUV_{lung}), mediastinal blood pool (SUV_{MBP}), and liver (SUV_{liver}) on both rest and stress images were calculated to be used as internal references, as previously described.[1] SUV_{fat} was calculated in the right and left upper and lower posterior chest walls, SUVlung in the right and left lower and upper lobes roughly midway between anterior and posterior chest walls, in areas free from abnormal CT findings, and SUV_{liver} in four areas roughly equidistant from left to right within the liver. ROI diameter was 1.5 cm for reference SUV_{max} calculations, adjusted to smaller sizes for SUVfat if needed. Results for both visual and semiquantitative analyses of individual lesions are shown in ►**Tables 1** and **2**. Ratios of tumor to various background tissues are shown in ►**Tables 3** and **4**.

Uptake in the lungs was noted visually to vary significantly between locations (a top-to-bottom and posterior-to-anterior gradient was noted), and so, specific data relating to position were calculated by a third observer. Data were obtained as described before in the apex (as far up as one could go without visible end-of-image noise), in the midlung (roughly at the carina), and in the anterior and posterior base of each lung.

Statistics

We used Cohen's kappa with linear weighting (using MATLAB, The MathWorks, Natick, Massachusetts, United States) to compare readers. We compared each reader to the other reader on both rest and stress images and a kappa statistic calculated. We calculated descriptive statistics on SUV_{max} for both rest and stress images separately, and used two-tailed two-sample paired *t*-tests (using Microsoft Excel 2016, Redmond, Washington, United States) to compare rest and stress values of SUV_{max}, for both breast and lung tumors. Two-tailed two-sample paired *t*-tests were also used to compare SUV_{max} of each patient's tumor with the average value of their normal structures, and two-tailed two-sample unpaired tests were used to compare the breast and lung cancer groups, as well as the receptor positive and negative groups for breast cancer patients. Too few lung cancer patients had receptor analysis done to make statistical studies possible.

Results

Visual Analysis

In 25 out of 53 patients, visual scores matched for both rest and stress images; in most other patients, readers disagreed by one category, though in three cases (rest) and five cases (stress), they disagreed by two categories. Reader 2 tended to have higher readings by approximately 0.4 on average. Cohen's kappa with linear weighting for readers 1 and 2 was 0.57 for rest and 0.50 for stress, indicating moderate agreement between observers.

Quantitative Analysis

SUV_{max} for breast cancer lesions ranged from 0.3 to 4.6, with an average of 1.6 (median 1.2, standard deviation [SD] 1.1); only three of these had FDG PET/CT, but SUV_{max} was 5.9, 19.0, and 21.0, showing the greater avidity of FDG PET/CT for breast cancer lesions. SUV_{max} for lung cancer lesions ranged from 0.8 to 6.3, with an average of 3.1 (median 3.0, SD 1.6); 21 of these had FDG PET/CT, and again lung cancers showed more avidity for FDG PET/CT with a range from 0.8 to 20.0, with average 9.4. In nearly all cases, SUV_{max} was higher for FDG PET/CT. Correlation coefficient between SUV_{max} for FDG and for Rb was 0.16, showing essentially no significant correlation. As a result, the possibility that Rb essentially "tracks with" FDG is excluded. Specificity is difficult to assess as no equivalent database of benign tumors exists (patients would be unlikely to be admitted for a known benign tumor.) As in our prior study, SUV_{max} was slightly higher at rest than at stress for both types of cancers (1.7 vs. 1.5 for breast and 3.2 vs. 3.0 for lung); the effect was not significant in either case ($p = 0.57$ breast and $p = 0.61$ lung). Lung values were significantly higher than breast values ($p < 0.0001$). Tumor values were significantly different from lung, fat, and liver ($p < 0.0001$), but interestingly not significantly different from blood pool ($p = 0.16$). However, subdividing this into comparing breast groups ($p = 0.005$) and lung groups ($p = 0.0002$) shows both groups have uptake in tumors significantly different from blood pool.

Average uptake was 2.4 for MBP (2.5 rest and 2.3 stress), 1.2 for lung (1.2 rest and 1.1 stress), 0.3 for chest wall (this did not vary), and 3.6 for liver (3.5 rest and 3.7 stress). (Note the distinction from FDG: most cancers were *less* avid than liver, used as a benchmark for low-grade uptake in cancers such as lymphoma.) Thus, there is a very slight movement from blood pool and lung (and tumors) into liver with stress imaging.

Location-indexed SUVs for background lung gave similar overall values (1.2 rest and 1.1 stress), with the left lung marginally more avid than the right (1.3 left and 1.2 right). Average uptake was 1.1 at the apex, 1.2 at the midlung, 1.1 at the anterior base, and 1.5 at the posterior base, confirming the general tendency of the lungs to accumulate tracer in dependent regions (►**Fig. 3**). As can be seen, lesions may be less avid than blood pool and similar to surrounding lung (►**Fig. 4**).

All breast cancer lesions had estrogen receptor (ER), progesterone receptor (PR), and human epidermal growth factor receptor type 2 (HER2) data available. Receptor data for lung cancer lesions was inconsistent as lesions were variably assessed over a period of 10 years which included considerable evolution in tests available and their use in oncologic practice, but histopathology was available in all cases. SUV_{max} averaged 0.8 for ER− and 1.8 for ER+ tumors (significant, $p = 0.0004$), 1.3 for PR+ and 1.8 for PR− tumors (not significant, $p = 0.15$), and 1.6 for HER2− and 1.4 for HER2+ tumors (not significant, $p = 0.54$). The ER result fits the thallium pattern of being higher in better-differentiated tumors (in this case breast cancer rather than lymphomas), though with such a small sample size, it is difficult to be

Table 1 Visual assessments and SUV_{max} of each identified lesion, stress, rest, and FDG: breast cancer

Cancer type	Visual score				Quantitative score (SUV_{max})		
	Rdr 1, rest	Rdr 1, stress	Rdr 2, rest	Rdr 2, stress	Rb (rest)	Rb (stress)	FDG
Triple neg	3	3	1	1	0.85	0.62	
Triple neg	2	2	1	1	0.63	0.52	
Triple neg	1	1	1	1	0.86	0.73	
HER2+	3	3	3	3	1.5	0.89	
ER+	2	2	2	2	1	0.92	
ER+	3	3	3	3	3.5	2.7	21
ER+ PR+	3	3	2	2	1.3	1.2	
ER+ PR+	2	2	3	2	1.5	1.2	
ER+ PR+	3	3	4	4	1	0.77	19
ER+ PR+	2	2	2	1	1.6	1.1	
ER+ PR+	3	3	3	2	1.5	1.8	
ER+ PR+	3	3	3	3	4.6	4.4	
ER+ PR+	2	2	1	1	2.6	2.4	5.9
Triple pos	2	2	2	2	1.1	1.1	
Triple pos	2	2	3	3	2.1	1.4	
Triple pos	3	3	3	3	2.6	2.9	
Triple pos	1	1	1	1	0.3	0.23	
Range	1–3	1–3	1–4	1–4	0.3–4.6	0.2–4.4	5.9–21
Mean ± SD	1–3	1–3	1–4	1–4	1.7 ± 1.1	1.5 ± 1.1	15.3 ± 8.2

Abbreviations: Adeno, adenocarcinoma; ER, estrogen receptor; FDG, fluorodeoxyglucose; HER2, human epidermal growth factor receptor type 2; PR, progesterone receptor; Rdr, reader; SCC, squamous cell carcinoma; SCLC, small cell lung cancer; SD, standard deviation; SUV_{max}, maximum standard uptake value; Triple neg, triple negative; Triple pos, triple positive.
Note: Blank entries for FDG are cases where no study was available.

definitive; still, the finding bears further study. For lung cancer, SUV_{max} averaged 3.3 for adenocarcinoma, 3.1 for squamous cell, and 3.1 for small cell, not significantly different. The six tumors with programmed death-ligand 1 mutations had SUV_{max} of 4.1 at rest and 4.0 at stress, but the others were not tested for this mutation.

Among the rarer tumors, the well-differentiated carcinoid had SUV_{max} 4.8 on average, the esophageal tumors 3.2 and 4.1, the ovarian carcinosarcoma 1.7, the lymphomas ranged from 1.2 to 2.8 (1.2 mantle cell, 2.5 follicular, 2.8 small lymphocytic lymphoma [SLL] and post-transplant lymphoproliferative disorder [PTLD]), the renal cell metastasis 0.92, and the GI metastasis 1.4.

Discussion

There was only moderate agreement between observers, from 0.50 to 0.56 Cohen's kappa with linear weighting. This is somewhat lower than agreement in the prior study, where recalculating Cohen's kappa with linear weighting gave agreements of 0.808 and 0.869. Collapsing categories 1 and 2 has only minimal effect (it rises to 0.61–0.64). The largest number of discrepancies at both rest and stress was between categories 2 and 3 (between fat and lung and between fat and mediastinum), and may reflect the considerable variability of uptake within the lung. This suggests that future benchmarks might include fat, MBP, and liver only if this form of grading is to be useful in the future. (It is worth noting that the Deauville scale comfortably uses MBP and liver alone.) Given the interobserver variability, however, it may not be useful as a primary imaging study in the oncologic setting. Instead, close attention should be paid to reviewing Rb cardiac scans for the presence of incidental tumors. While our study was "enriched" in incidental tumors as a result of the patients being specifically selected for having had a tumor found, the usual previously described 2% incidental cancer discovery rate[8] still suggests this is an important incidental finding to beware of.

Values are relatively similar at rest and stress. This is compatible with a prior case report of two patients with metastases detected on a Rb scan which showed little response to adenosine.[9] Of course, this case report uses a different agent and a very small sample size. Nonetheless, it does confirm that vasodilation does not significantly affect tumor perfusion (all stress tests in this study used regadenoson).

Table 2 Visual assessments and SUV_{max} of each identified lesion, stress, rest, and FDG: lung cancer

Cancer type	Visual score				Quantitative score (SUV_{max})		
	Rdr 1, rest	Rdr 1, stress	Rdr 2, rest	Rdr 2, stress	Rb (rest)	Rb (stress)	FDG
Adeno	3	3	4	4	6	5.4	
Adeno	3	3	3	3	4	2.5	
Adeno	1	1	1	1	0.8	1	0.82
Adeno	2	2	2	1	1.6	1.5	
Adeno	2	2	2	2	1.2	1.1	
Adeno	3	3	3	3	3.5	2.6	4.6
Adeno	3	3	3	2	2.3	1.6	2.1
Adeno	1	1	2	2	0.81	0.85	2.2
Adeno	2	2	3	3	2.5	4.8	10
Adeno	4	4	4	4	6.3	6.4	7.9
Adeno	4	3	3	4	4.2	2.8	15
Adeno	3	3	3	3	3.7	3.2	10
Adeno	2	2	2	2	0.97	0.7	2.1
Adeno	3	3	3	3	4.7	3.8	20
Adeno	3	3	4	4	4.5	4.6	14
Adeno	3	2	3	2	5.6	7.8	12
Adeno	4	4	4	4	5.8	4.8	
Adeno	2	2	2	2	1.6	1.3	
Adeno	3	3	2	2	2.6	2.3	
SCC	4	4	3	3	4.3	4.9	
SCC	2	2	2	2	2.5	2	
SCC	3	3	4	3	3.8	3.3	14
SCC	3	3	3	3	3.6	3	6.6
SCC	2	2	2	2	3.4	3.4	
SCC	3	3	3	3	3	2.6	10
SCC	3	3	3	3	1.8	1.9	10
SCC	4	4	4	3	5.2	3.5	
SCC	3	3	3	3	2.1	2.3	3.7
SCC	4	4	4	3	1.9	2.4	
SCLC	3	3	3	3	3.9	3.3	
SCLC	4	4	3	3	5.5	5.1	17
SCLC	3	3	3	3	2.5	2.7	
SCLC	3	3	2	2	2.9	3.6	
SCLC	1	1	4	4	4	3.5	7.6
SCLC	4	4	4	4	1.8	1.7	8.6
SCLC	3	3	3	3	1.6	1.3	20
Range	1–4	1–4	1–4	1–4	0.8–6.3	0.7–7.8	0.82–20
Mean ± SD	n/a	n/a	n/a	n/a	3.2 ± 1.6	3.0 ± 1.6	9.4 ± 5.8

Abbreviations: Adeno, adenocarcinoma; FDG, fluorodeoxyglucose; n/a, not available; Rdr, reader; SCC, squamous cell carcinoma; SCLC, small cell lung cancer; SD, standard deviation; SUV_{max}, maximum standard uptake value.
Note: Blank entries for FDG are cases where no study was available.

Table 3 SUV_{max} (Rb rest and stress) ratios to fat, lung, MBP, and liver: breast cancer

Cancer type	Rest/fat	Stress/fat	Rest/lung	Stress/lung	Rest/MBP	Stress/MBP	Rest/liver	Stress/liver
Triple neg	2.4	1.8	0.6	0.4	0.3	0.2	0.2	0.2
Triple neg	2.7	2.2	0.9	0.7	0.3	0.3	0.3	0.2
Triple neg	2.9	2.5	0.4	0.3	0.2	0.2	0.2	0.1
HER2+	6.3	3.7	1.3	0.8	0.9	0.6	0.3	0.2
ER+	4.2	3.8	0.8	0.8	0.5	0.5	0.4	0.3
ER+	8.4	6.5	2.0	1.5	1.3	1.0	0.6	0.5
ER+ PR+	6.8	6.3	4.1	3.8	1.2	1.1	0.7	0.6
ER+ PR+	4.4	3.5	0.9	0.7	0.7	0.5	0.4	0.3
ER+ PR+	12.7	9.8	2.4	1.9	1.3	1.0	1.0	0.8
ER+ PR+	4.5	3.1	1.0	0.7	0.7	0.5	0.3	0.2
ER+ PR+	11.4	13.7	2.8	3.4	1.1	1.3	0.8	0.9
ER+ PR+	15.3	14.6	2.1	2.0	1.3	1.2	1.0	1.0
ER+ PR+	7.9	7.3	0.7	0.7	0.6	0.6	0.6	0.5
Triple pos	4.5	4.5	1.0	1.0	0.4	0.4	0.3	0.3
Triple pos	9.2	6.1	2.2	1.4	0.9	0.6	0.6	0.4
Triple pos	5.3	5.9	1.8	2.1	0.8	0.9	0.5	0.6
Triple pos	1.2	0.9	0.2	0.1	0.1	0.1	0.1	0.1
Range	1.2–15.3	0.9–14.6	0.2–4.1	0.1–3.8	0.1–1.3	0.1–1.3	0.1–1.0	0.1–1.0
Mean ± SD	6.5 ± 3.9	5.7 ± 3.9	1.5 ± 1.0	1.3 ± 1.0	0.8 ± 0.4	0.6 ± 0.4	0.5 ± 0.3	0.4 ± 0.3

Abbreviations: Adeno, adenocarcinoma; ER, estrogen receptor; FDG, fluorodeoxyglucose; HER2, human epidermal growth factor receptor type 2; MBP, mediastinal blood pool; PR, progesterone receptor; Rb, rubidium; Rdr, reader; SCC, squamous cell carcinoma; SCLC, small cell lung cancer; SD, standard deviation; SUV_{max}, maximum standard uptake value; Triple neg, triple negative; Triple pos, triple positive.

There is a substantial amount of variability in tumor-to-background ratios, whether lung, fat, MBP, or liver is used. Descriptive statistics in ►**Tables 3** and **4** suggest a high degree of variation relative to the mean for most ratios. Again, breast tumors are less avid than many background lesions, whereas lung tumors are more avid than fat, blood pool, and lung, but still less avid than normal liver.

There is little correlation between intensity and histology or receptor status, with the interesting exception of ER+ tumors being more Rb avid. While this is an intriguing result, raising the possibility of being able to assess tumors for ER status using existing tracers (rather than tracers such as fluoroestradiol which are difficult to manufacture), it is based on a small sample size and would require confirmation in a larger dataset. Since almost all ER+ tumors had an expression level of 91 to 100%, any sort of quantitative dose–response relationship is difficult to ascertain.

The role of perfusion is another open question. Rb's primary purpose in nuclear imaging is to be used in the heart as a perfusion tracer, after all. Common intravenous contrast does assess perfusion, but additional contrast-enhanced CT images were not available pretreatment or even posttreatment on most of these patients, as our institution usually performs dedicated CTs of the chest without contrast. Only approximately 15 had such scans, and the protocol of the CT varied between venous-phase cancer staging CTs and pulmonary-arterial-phase CTs for pulmonary embolus detection.

Rb is most similar pharmacologically to thallium, which the cell also transports inside via the sodium–potassium exchange transporter, and which was investigated as a tumor agent in the late 1980s and early 1990s. Histopathologic data on Na^+/K^+ ATPase is not available, as this is a retrospective study and this is not commonly assessed in clinical practice. Correlation of thallium uptake with grade is inconsistent. While a higher uptake correlates with a worse prognosis in lung cancer and sensitivity better for poorly differentiated lung cancers,[10,11] thallium is more sensitive in *low*-grade lymphomas,[10,11] though it may be even more so in intermediate-grade lymphomas.[12] As thallium tumor studies were usually minutes to hours after injection rather than immediately after injection for ^{82}Rb,[10–14] the physiology may be very different in any case. Nonetheless, despite the inconsistent correlation of thallium with tumor differentiation, the possibility of a correlation of Rb with ER activity bears further study.

Table 4 SUV_{max} (Rb rest and stress) ratios to fat, lung, MBP, and liver: lung cancer

Cancer type	Rest/fat	Stress/fat	Rest/lung	Stress/lung	Rest/MBP	Stress/MBP	Rest/liver	Stress/liver
Adeno	28.0	25.2	4.4	3.9	2.0	1.8	1.2	1.1
Adeno	14.1	8.8	3.3	2.1	1.6	1.0	0.9	0.6
Adeno	5.1	6.4	1.1	1.3	0.4	0.5	0.2	0.3
Adeno	5.0	4.7	1.4	1.3	0.7	0.7	0.4	0.4
Adeno	7.5	6.9	1.6	1.4	0.5	0.5	0.3	0.3
Adeno	14.5	10.8	2.2	1.6	1.7	1.2	1.0	0.7
Adeno	4.4	3.0	4.2	2.9	1.1	0.7	0.9	0.6
Adeno	1.4	1.5	1.2	1.3	0.5	0.5	0.4	0.4
Adeno	10.9	20.9	1.8	3.4	1.2	2.3	0.8	1.5
Adeno	10.7	10.9	4.3	4.4	1.7	1.7	1.3	1.4
Adeno	10.0	6.7	5.1	3.4	2.0	1.3	1.3	0.9
Adeno	10.0	8.6	4.2	3.6	1.3	1.1	0.9	0.8
Adeno	3.4	2.5	2.0	1.5	0.6	0.5	0.4	0.3
Adeno	15.3	12.4	2.6	2.1	2.4	1.9	1.3	1.0
Adeno	15.7	16.0	3.1	3.1	1.7	1.7	1.0	1.0
Adeno	10.5	14.6	6.2	8.7	1.3	1.8	1.0	1.4
Adeno	24.5	20.2	5.9	4.9	2.4	2.0	1.3	1.1
Adeno	3.8	3.1	2.2	1.8	0.7	0.5	0.6	0.5
Adeno	10.6	9.4	1.4	1.2	1.0	0.9	0.8	0.7
SCC	12.3	14.1	3.1	3.6	1.5	1.7	0.9	1.0
SCC	4.4	3.5	4.1	3.3	1.3	1.1	1.0	0.8
SCC	11.3	9.8	3.8	3.3	1.7	1.5	1.0	0.9
SCC	6.4	5.3	2.4	2.0	1.3	1.1	0.7	0.6
SCC	9.2	9.2	1.8	1.8	1.3	1.3	0.8	0.8
SCC	5.9	5.1	5.6	4.9	1.3	1.2	0.7	0.6
SCC	4.9	5.2	2.6	2.8	1.0	1.1	0.6	0.6
SCC	17.7	11.9	4.9	3.3	1.8	1.2	1.4	0.9
SCC	7.0	7.7	2.7	2.9	1.8	2.0	0.8	0.8
SCC	8.0	10.1	2.7	3.4	1.1	1.3	1.0	1.2
SCLC	16.2	13.7	1.8	1.6	1.5	1.3	1.0	0.8
SCLC	16.9	15.7	2.7	2.5	1.5	1.4	1.3	1.2
SCLC	6.8	7.4	3.6	3.9	1.6	1.7	0.9	1.0
SCLC	7.7	9.5	2.4	3.0	0.7	0.9	0.6	0.8
SCLC	19.9	17.4	3.4	3.0	1.6	1.4	1.3	1.1
SCLC	12.7	12.0	3.2	3.0	1.4	1.4	1.3	1.2
SCLC	5.6	4.6	4.7	3.8	1.7	1.4	0.8	0.7
Range	1.4–28.0	1.5–25.2	1.1–6.2	1.2–8.7	0.4–2.4	0.5–2.3	0.2–1.4	0.3–1.5
Mean ± SD	10.5 ± 6.0	9.8 ± 5.6	3.2 ± 1.4	2.9 ± 1.4	1.4 ± 0.5	1.3 ± 0.5	0.9 ± 0.3	0.8 ± 0.3

Abbreviations: Adeno, adenocarcinoma; FDG, fluorodeoxyglucose; MBP, mediastinal blood pool; Rdr, reader; SCC, squamous cell carcinoma; SCLC, small cell lung cancer; SD, standard deviation; SUV_{max}, maximum standard uptake value.

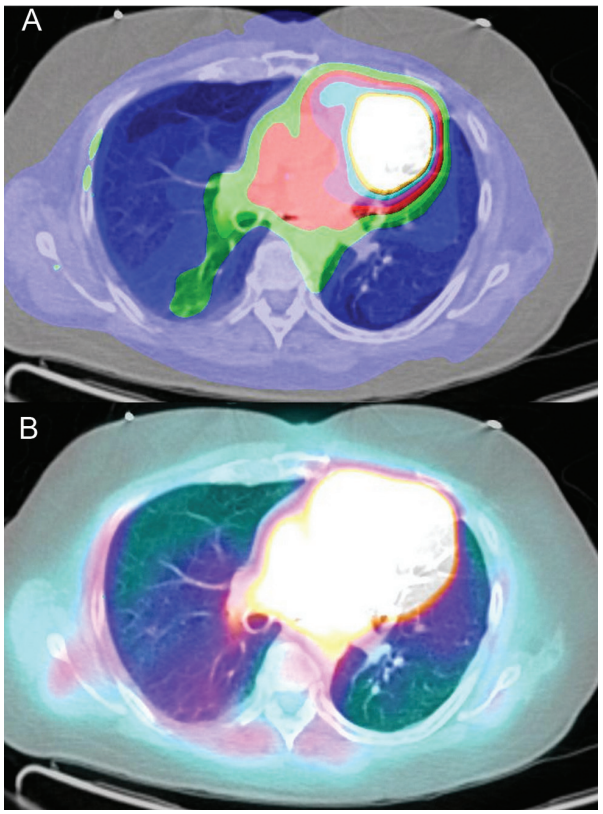

Fig. 3 (**A**, **B**) Dependent accumulation of tracer in the lung (*rest image*). The changes of three steps in the top image (each representing 0.25) indicates a difference of at least 0.75 between parts of the lung.

Conclusion

Malignant tumors can be depicted and quantified on ^{82}Rb PET/CT; while uptake is low relative to FDG PET/CT, and interobserver variability suggests it is not useful as a primary oncologic imaging modality, early findings involving receptors suggest further investigation is needed to see if it can be useful as a form of molecular imaging.

Authors' Contribution

J.D.O. designed the study, helped in literature search, data acquisition, data analysis, statistical analysis, manuscript preparation, and was the guarantor. A.D.F. and M.A.M. contributed to data acquisition and manuscript preparation. A.H.K. contributed to concept and manuscript preparation. All authors read and approved the final manuscript, requirements for authorship have been met, and each author believes manuscript represents honest work.

Funding

None.

Conflict of Interest

None declared.

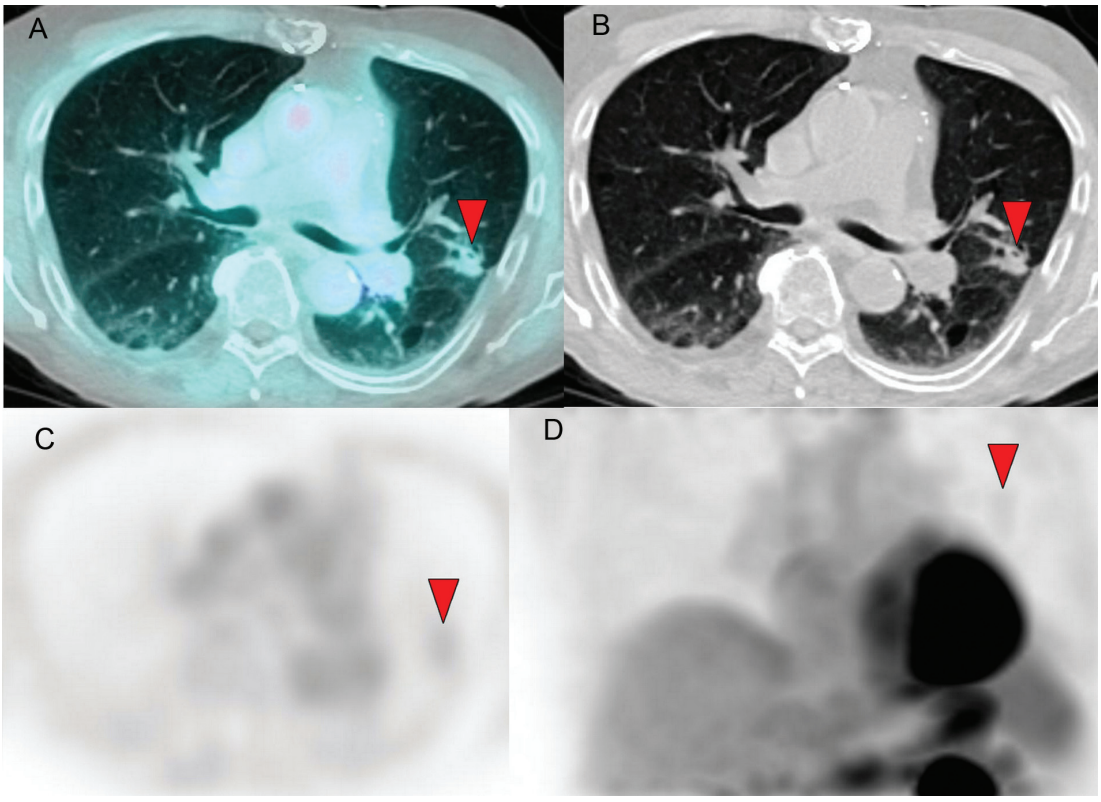

Fig. 4 (**A**–**D**) Less avid lung lesion (*red arrowhead*) on rest image, less avid than mediastinal blood pool and similar to surrounding lung.

References

1 Khandani AH, Commander CW, Desai H, et al. Visual and semi-quantitative analysis of ^{82}Rb uptake in malignant tumors on PET/CT: first systematic analysis. Nucl Med Commun 2019;40 (05):532–538

2 Roelcke U, Radü E, Ametamey S, Pellikka R, Steinbrich W, Leenders KL. Association of rubidium and C-methionine uptake in brain tumors measured by positron emission tomography. J Neuro-oncol 1996;27(02):163–171

3 Roelcke U, Radü EW, Hausmann O, Vontobel P, Maguire RP, Leenders KL. Tracer transport and metabolism in a patient with juvenile pilocytic astrocytoma. A PET study. J Neurooncol 1998;36 (03):279–283

4 Neumann DR, Basile KE, Bravo EL, Chen EQ, Go RT. Malignant pheochromocytoma of the anterior mediastinum: PET findings with [18F]FDG and ^{82}Rb. J Comput Assist Tomogr 1996;20(02): 312–316

5 Gupta A, DiFilippo FP, Brunken RC. Rubidium-82 uptake in metastases from pheochromocytoma on PET myocardial perfusion images. Clin Nucl Med 2011;36(10):930–931

6 Lu Y. FDG and (82)Rb PET/MRI features of brain metastasis of breast cancer. Clin Nucl Med 2015;40(06):494–495

7 Jochumsen MR, Tolbod LP, Pedersen BG, et al. Quantitative tumor perfusion imaging with (82)rubidium-PET/CT in prostate cancer - analytical and clinical validation. J Nucl Med 2019;60(08): 1059–1065

8 Mirpour S, Khandani AH. Extracardiac abnormalities on rubidium-82 cardiac positron emission tomography/computed tomography. Nucl Med Commun 2011;32(04):260–264

9 Hasbak P, Enevoldsen LH, Fosbøl MO, Skovgaard D, Knigge UP, Kjær A. Rubidium-82 uptake in metastases from neuroendocrine tumors: no flow response to adenosine. J Nucl Cardiol 2016;23(04):840–842

10 Roach PJ, Cooper RA, Arthur CK, Ravich RB. Comparison of thallium-201 and gallium-67 scintigraphy in the evaluation of non-Hodgkin's lymphoma. Aust N Z J Med 1998;28(01):33–38

11 Waxman AD, Eller D, Ashook G, et al. Comparison of gallium-67-citrate and thallium-201 scintigraphy in peripheral and intrathoracic lymphoma. J Nucl Med 1996;37(01):46–50

12 Mansberg R, Wadhwa SS, Mansberg V. Tl-201 and Ga-67 scintigraphy in non-Hodgkin's lymphoma. Clin Nucl Med 1999;24(04): 239–242

13 Takekawa H, Takaoka K, Tsukamoto E, Kanegae K, Miller F, Kawakami Y. Thallium-201 single photon emission computed tomography as an indicator of prognosis for patients with lung carcinoma. Cancer 1997;80(02):198–203

14 Takekawa H, Itoh K, Abe S, et al. Thallium-201 uptake, histopathological differentiation and Na-K ATPase in lung adenocarcinoma. J Nucl Med 1996;37(06):955–958

